Research Square

Preprints are preliminary reports that have not undergone peer review.
They should not be considered conclusive, used to inform clinical practice,
or referenced by the media as validated information.

Resolving the aragonite (CaCO3) superstructure paradox

Vesna Ribić
Jožef Stefan Institute
Zsombor Molnár
University of Pannonia
Péter Pekker
University of Pannonia
Péter Németh
Institute for Geological and Geochemical Research
István Dódony
University of Pannonia
Mihály Pósfai
University of Pannonia
Pavel Gavryushkin
V.S. Sobolev Institute of Geology and Mineralogy
Aleksander Rečnik
aleksander.recnik@ijs.si

Jožef Stefan Institute

Article

Keywords:

Posted Date: July 10th, 2026

DOI: https://doi.org/10.21203/rs.3.rs-10189142/v1

License: This work is licensed under a Creative Commons Attribution 4.0 International License.
Read Full License

Additional Declarations: No competing interests reported.

Resolving the aragonite ($CaCO_3$) superstructure paradox

*Vesna Ribić,[1] Zsombor Molnár,[2,3] Péter Pekker,[2] Péter Németh,[2,4] István Dódony,[2] Mihály Pósfai,[2,3] Pavel N. Gavryushkin[5] and Aleksander Rečnik[1]**

[1] Jožef Stefan Institute, Department for Nanostructured Materials, Ljubljana (Slovenia)
e–mail: aleksander recnik@ijs.si (the Corresponding Author).

[2] University of Pannonia, Research Institute of Biomolecular and Chemical Engineering, Nanolab, Veszprém (Hungary).

[3] HUN-REN-PE Environmental Mineralogy Research Group, Veszprém (Hungary).

[4] Institute for Geological and Geochemical Research, HUN-REN Research Centre for Astronomy and Earth Sciences (MTA Centre of Excellence), Budapest (Hungary).

[5] V.S. Sobolev Institute of Geology and Mineralogy, Siberian Branch of Russian Academy of Sciences, Novosibirsk (Russia).

* The corresponding author email: aleksander.recnik@ijs.si

ARTICLE HIGHLIGHT *Ghost polytypes inferred from superstructure and symmetry–forbidden reflections in biogenic, geological, speleothem and synthetic aragonite are disputed. Reflection artifacts in aragonite are shown to arise from nanoscale twinning providing a unified framework for identifying similar diffraction anomalies in other multiply twinned materials.*

Abstract. Mysterious superstructure and symmetry–forbidden reflections seen across biogenic, geological, speleothem, and synthetic aragonite, regardless of composition or growth conditions, that have long fueled speculations about new $CaCO_3$ polytypes are explained by nanoscale twinning. Using classical electron diffraction and structure modeling, we show that these reflections result from double diffraction signatures of polysynthetic twinning. Due to inherently nonperiodic character and associated structural complexity, nanoscale twinning is rarely considered in interpretation of diffraction artifacts arising in non edge–on projections. We demonstrate that false diffraction signatures, which closely mimic hypothetical superstructures, arise from coincident lattice sites through which the twin domains are linked. They are seen only in projections where the twin boundaries are inclined with respect to electron beam. The origin of false reflections by twinning is validated via crystallographic matrix analysis, simulations of dynamic electron–wave scattering through inclined interfaces via twin-based supercell approximations, and is proved by high-angle tilting experiments that directly link half-integer reflections with intrinsic twinning. Our study reconciles decades of conflicting observations and establishes intrinsic twinning as the root cause of false superstructure reflections in aragonite, and moreover, it provides a generalized framework for identification of twin–related diffraction artifacts hinting at unknown phases in other twinned materials, such as martensitic steels and semiconductors.

1. Introduction

Aragonite is a widespread crystalline form of $CaCO_3$ and one of the most frequently occurring biominerals on the Earth surface.[1] While the crystal structure of aragonite was solved a century ago by Lawrence Bragg (1924),[2] there are still several features in diffraction patterns that remain a challenge to crystallographers. Ideally, the aragonite structure belongs to the *Pmcn* space group. However, many studies report the presence of reflections that should be systematically absent, lowering the aragonite symmetry to a triclinic $P\bar{1}$.[3] While the changes in structure factors of the forbidden reflections can be explained by impurities or point defects,[3,4] additional, superstructure reflections, with no simple explanation are often observed.

A particularly puzzling reciprocal lattice problem was pointed out in electron microscopy and X–ray diffraction study of synthetic aragonite by Hiragi *et al*. in 1966.[5] The authors observed unusual reflection maxima with half–integer indices ½½*l*, suggesting the existence of a yet unknown superstructure of aragonite. They reconstructed this condition by periodic twinning of aragonite on every (110) layer and described the new structure within the *Pbca* space group (a=8.420, b=9.385, c=5.741 Å) that adequately explains the observed condition. Unaware of Hiragi's work, Makovicky (2012)[6] predicted a two–layered twin–based *Pcab* polytype, using order–disorder (OD) approach, and arrived to similar conclusions as Hiragi *et al*.[5] Despite the fact that {110} twinning is a common structural feature of all known low–pressure aragonite samples, including geological,[2–4,7–13] biogenic,[14–43] and synthetic,[5,44–52] some authors argued that two–layered twin–based *Pcab* polytype is unlikely to exist due to high desymmetrization of aragonite structure,[6] and was never considered plausible in further theoretical studies of aragonite.[53–57]

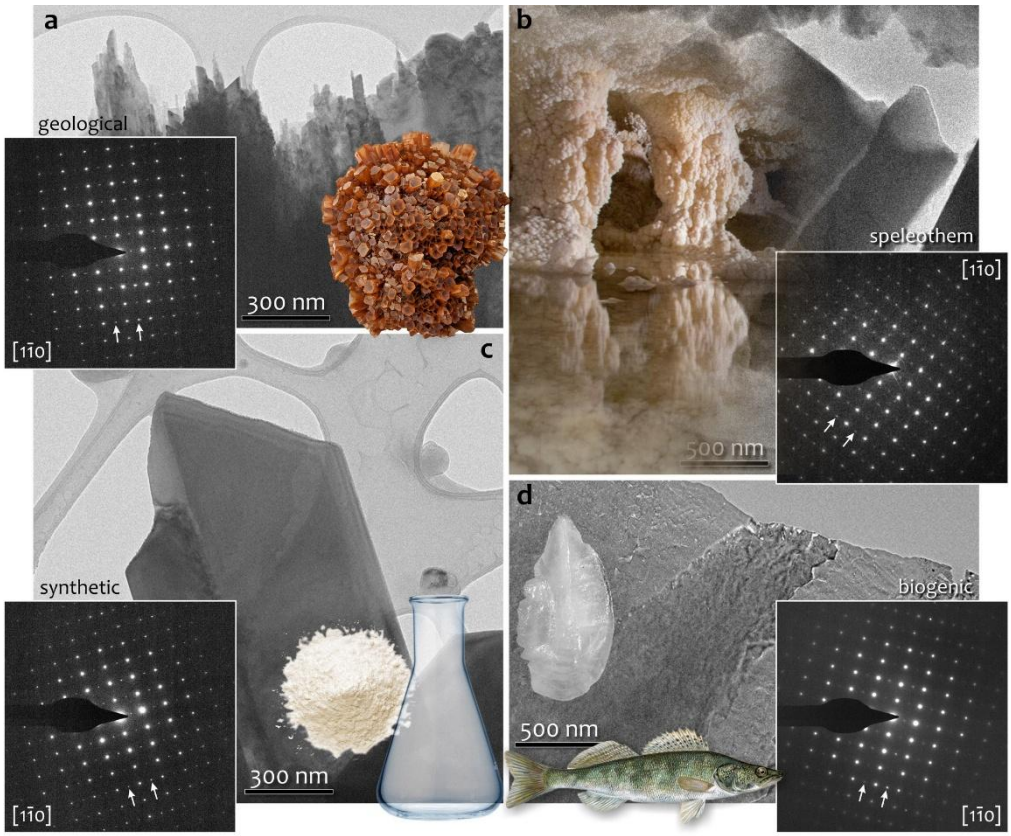


Fig. 1: **Apparent superstructure reflections in aragonite specimens of various origin**. (**a**) Geological; pseudohexagonal {110} twinned aragonite crystals from Tazouta, Morocco. (**b**) Speleothem; aragonite from Berger Károly cave, Hungary. (**c**) Synthetic; nanocrystalline aragonite precipitated from Na_2CO_3+$CaCl_2$ solutions, (**d**) Biogenic; fish otolith (*Sander lucioperca*). The arrows indicate rows of half–integer (*h*+½, *k*+½, *l*) reflections that can not be indexed within the *Pmcn* space group of aragonite. Photographs of objects are illustrative and do not represent the actual samples.

Diffraction experiments on various aragonite samples typically show reflections that can not be simply attributed to dynamic scattering. Among these, half–integer (h+½ k+½ l) HM–type reflections* in ⟨110⟩ projections appear to be a recurring feature of electron diffraction patterns of virtually any low–pressure aragonite sample, as demonstrated in Fig. 1. Besides synthetic aragonite studied by Hiragi *et al*. (1966; Fig. 1),[5] the HM type reflections have been recorded in lacustrine stromatolites (Fig. 3c; Benzerara *et al*. 2010)[18], bivalve shells (Fig. 5b; Hayashi *et al*. 2011),[23] synthetic aragonite mesocrystals (Fig. 2d; Yu *et al*. 2017)[49] carbonate precipitates from the speleothems (Fig. 2; Németh *et al*. 2018)[8] and pseudohexagonal aragonite crystals from different mineralogical deposits (Fig. 1; Gavryushkin *et al*.[9]). More specifically, Németh *et al.* (2018) reported that half–integer reflections are result of diffuse scattering that can be explained by the presence of the newly discovered 6–layered monoclinic aragonite (*mAra*), that forms as a precursor of the conventional *Pmcn* aragonite in speleothems. Using electron diffraction tomography on best–ordered crystals, they identified *mAra* as monoclinic with space group $P2_1/c$. Ab–initio structure solution showed that *mAra* has a layered aragonite structure consisting of 6 {110} slabs (layers). *mAra* could contain a significant amount of Mg atoms and –OH groups. Further, they suggested that with its twin elements *mAra* is the possible cause of (110) twinning in aragonite. Gavryushkin *et al.* (2024)[13] addressed the problem of local symmetry deviations in aragonite and suggested that (110) twins and stacking faults may be formed as a result of local strain compensation.

Our study investigates the origin of superstructure reflections in aragonite, a phenomenon that has puzzled researchers for more than half a century. Samples of aragonite from geological, speleothem, synthetic, and biogenic origins are studied, and show, that the apparent superstructure reflections are a common feature across all examined materials. An original methodology is developed that explains the emergence of these reflections through the application of electron diffraction techniques, structure modeling, and computational methods.

2. **Results and Discussion**

To address the issue of mysterious superstructure reflections in aragonite, samples from all known sources, where aragonite is identified to form under low–pressure conditions, were collected, and investigated using electron diffraction techniques complemented by structure modeling, quantum chemical calculations, and dynamical simulations of electron scattering.

2.1. **The occurrence of half–integer reflections in aragonite**.

HM reflections are observed in all samples investigated in this study (*cf.* Fig. 1), suggesting that this diffraction phenomenon is quite widespread and can be observed in aragonite samples of geological, speleothem, synthetic, as well as of biogenic origin. [$1\bar{1}0$] diffraction patterns with HM reflections can be readily indexed assuming the *Pcab* (n=1) polytype.[6] The characteristic appearance of the HM reflections as observed in ⟨110⟩–type projections of aragonite is shown in Fig. 2, where the ideal diffraction pattern of aragonite (Fig. 2a) is compared to the one with the unexplained HM reflections (Fig. 2b) and calculated electron diffraction pattern (Fig. 2c) for equivalent projection of the *Pcab* polytype[5,6] that perfectly reproduces the half–integer reflections. Are we dealing with a new polytype of aragonite, or some yet unexplained diffraction artifact? On the other hand, except for apparent half–integer reflections in this projection, the presence of this polytype could not be confirmed in HRTEM images or diffraction patterns in [001] projection of aragonite, which should show half–integer {110}–type superstructure reflections,

* In courtesy of the pioneering researchers studying superstructure reflections in aragonite, Hiragi *et al.* (1966)[5] and Makovicky (2012)[6] the {110} twin–based *Pcab* polytype will be referred to as a Hiragi–Makovicky (HM) polytype, whereas the corresponding half–integer {½,½,*l*} reflections are called the Hiragi–Makovicky (HM) reflections.

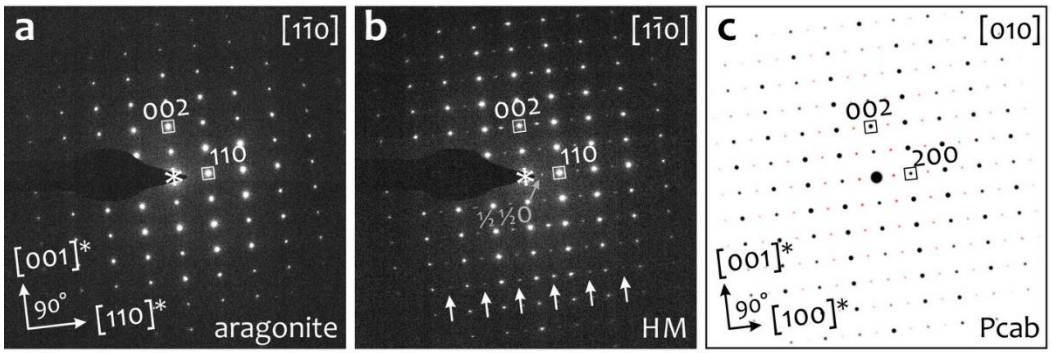


Fig. 2: **A new polytype of aragonite?** Electron diffraction patterns in [1$\bar{1}$0] projection of (**a**) ideal aragonite and (**b**) aragonite with an unexplained half–index superstructure reflections, indicated by arrows. The two patterns stem from the same crystal. (**c**) Calculated electron diffraction pattern of {110} twin–based *Pcab* polytype of aragonite in equivalent projection.[5,6] Regular reflections are indicated in *black* and the forbidden reflections in *red*. The match with the *Pcab* polytype is excellent; 100 reflection of the *Pcab* polytype corresponds to the ½½0 reflection condition. Experimental diffraction patterns were recorded from an aragonite crystal from Sefrou near Tazouta, Morocco.

and symmetrized {1$\bar{3}$0} lattice planes.[6] So the question arises why diffraction patterns of aragonite in [001] projection never show superstructure reflections, that should be observed, if this polytype of aragonite actually existed, and would be as common as the HM reflections (Appendix A, Fig. A1). Given the fact that disordered polysynthetic twins with short repeating distances are often observed,[5,9,13,19–25,30] it might be possible that the *Pcab* polytype exists in form of thin lamellae within twinned aragonite. While we observe such situations in HRTEM images, the boundary between regular aragonite and domains displaying half–integer reflections is not sharp, but diffuse, and the transition from one to another pattern is gradual (Fig. 3), suggesting that the actual interface between the two domains is not edge–on in this projection.

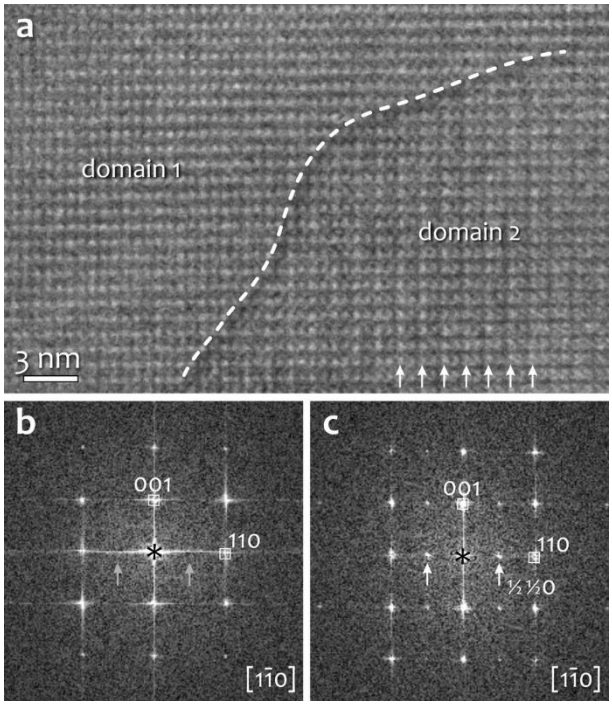


Fig. 3: **The origin of half–integer HM reflections in aragonite**. (**a**) HRTEM image of an aragonite crystal (Tuva) in [1$\bar{1}$0] projection displaying a transition between regular aragonite (domain 1; FFT in **b**, grey arrows – flat at ½½0 condition), and aragonite with double periodicity (domain 2; FFT in **c**, white arrows – sharp maxima emerging at ½½0 condition).

A thorough analysis of published high–resolution TEM data on aragonite also does not show evidence of polytypic ordering, casting a doubt on the true existence of the *Pcab* polytype, leaving these mysterious structural complexities, which are so commonly observed in aragonite, unexplained. In addition, the intensity of $00l|_{l=\text{odd}}$ reflections is unexpectedly high given the fact that this condition is forbidden by the *Pmcn* space group of aragonite, as well as by the *Pcab* space group of the *n*=1 polytype. While the half–integer reflections remain unexplained, possible reasons for the increased intensity of the $00l|_{l=\text{odd}}$ reflections include dynamic scattering, presence of impurities, or a breakdown of aragonite symmetry.

2.2. **The co–occurrence of ⟨110⟩ and ⟨100⟩ orientations**.

When studying the HM reflections, we often observe a co–occurrence of contiguous domains, where one is oriented in $[1\bar{1}0]$ projection, and the other is close to [100]. The transition between the two projections is smooth and accompanied with transient appearance of half–integer reflections. This observation suggests, that rather than the *Pbca* polytype of aragonite, as suggested by Hiragi *et al*. (1966),[5] these reflections could be produced by overlapping aragonite domains, that are linked through a specific orientation relationship. One of such situations is recorded on aragonite from a fish otolith sample, oriented in $[1\bar{1}0]$ projection (Fig. 4). At first glance, the lattice

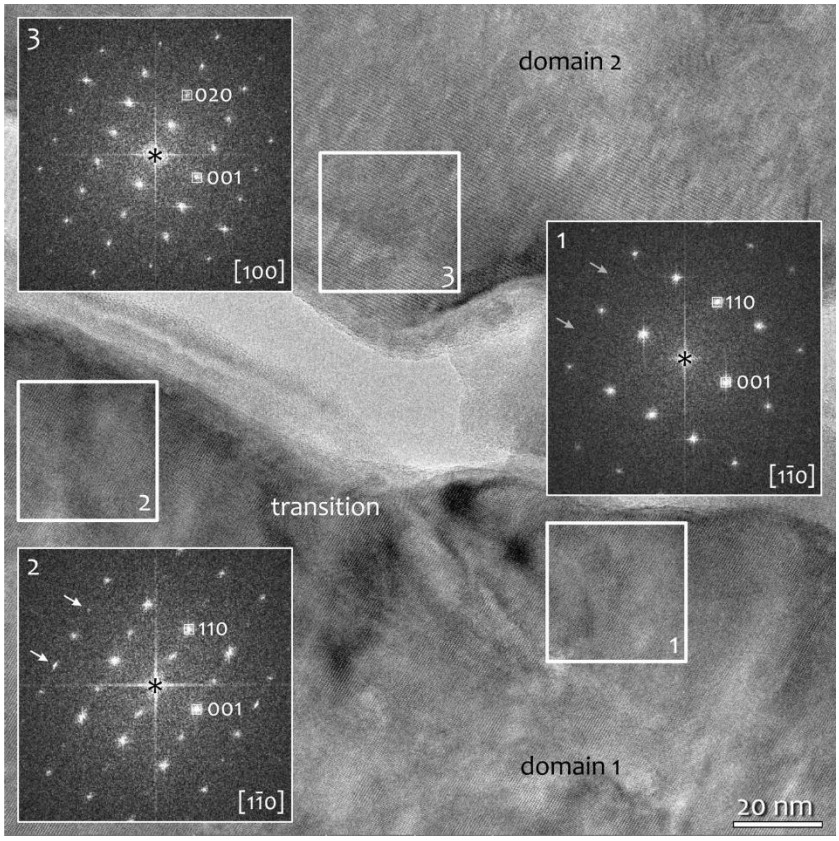


Fig. 4: **Co–occurrence of $[1\bar{1}0]$ and [100] projections** in fish otolith sample, a phenomenon indicating a specific crystallographic relationship between the two domains. The arrows in the FFT pattern (2) indicate the presence of HM reflections in the transition zone between domains 1 and 2.

image appears continuous, with no apparent orientation change. FFTs from different parts of the HRTEM image differ significantly, in one area (loc. 1) the diffraction pattern is trivial, and can be indexed with $[1\bar{1}0]$ of aragonite, slightly away from that position half–integer reflections start to appear (loc. 2), and further on, without a distinct interface in this orientation, a new projection emerges (loc. 3), that can be indexed as [100]. In this transition the orientation of the c–axis

remains roughly the same, only the projection gradually changes from [$1\bar{1}0$] to [100]. The co–occurrence of the two projections, identical orientation of the c–axis and the transition accompanied by the appearance of the half–integer reflections, are indicative of crystallographically related domains with an interface inclined with respect to the viewing direction.

Further, in diffraction patterns with HM reflections that are slightly off the [$1\bar{1}0$]–axis, we often observe splitting of high–index *hhl* reflections. No such splitting would be produced if the originating structure were the *Pbca* polytype, however, splitting would be present if the pattern stemmed from overlapping domains with similar lattice spacings, such as (110) with d=4.21 Å and (020) with d=3.98 Å, of [$1\bar{1}0$] and [100] projections, respectively. With only 6% difference in lattice spacings it can be expected that [$1\bar{1}0$] projections with HM reflections are misindexed as [100] projection and the unusual superstructure reflections are frequently overlooked.[49] For more clarification *see* Appendix, Fig. A2.

2.3. **HM reflections produced by (110) twinning of aragonite**.

While the *Pbca* (n=1) polytype that could explain the appearance of half–integer reflections has never been confirmed to exist in aragonite,[6] {110} twins, on the other hand, are abundantly present in aragonite crystallizing near ambient conditions.[19–43] The question then arises whether twinning could cause the HM reflections? Besides their random occurrence, {110} twins involve the exact same lattice translation as used to construct the *Pbca* polytype,[5,6] and are thus likely to produce similar diffraction conditions as the hypothetical polytype. There are two ways to verify this proposition. The first approach involves simulation of electron diffractions through aragonite domains related by twin operation in projections, such as [110], where the twin boundary is not parallel to the electron beam. The second approach would rely on physical tilting of (110)–twinned aragonite crystal from [001] projection, where the twins are easily identified, into [110] projection and experimentally confirm whether the problematic HM reflections indeed stem from the inclined twin boundaries. Neither of these approaches is easily accomplished; while the first one implies a calculation of the electron wave propagation through a nonperiodic crystal, the second one necessitates a physical crystal tilting of as much as 90°.

Let us first consider the crystallographic approach. According to the (110) twin model of aragonite, first proposed by Bragg (1924),[2] the relation between twin domains, D1 and D2, can be produced by 180° rotation around the (110)–plane normal after any chosen CO_3 layer. Crystallographically, the translation can be approximated by transformation matrix, **T**:

$$\mathrm{D1} \cdot \mathbf{T} = \mathrm{D2} \;;\; \mathbf{T} = \begin{pmatrix} 4/9 & 13/9 & 0 \\ 5/9 & -4/9 & 0 \\ 0 & 0 & 1 \end{pmatrix} \dagger \qquad (1)$$

Using this transformation matrix the orientation of the second twin domain D2 can be calculated for any given crystallographic projection of D1. For example, if domain D1 is oriented in [110] projection, the resulting orientation of D2 is [17/9 1/9 0]. Correspondingly, the relationship between the lattice planes and corresponding reflections is obtained by transposing **T** into **T**'.

To reconstruct the problematic [110] diffraction pattern of aragonite we start from the [001] projection, where the twin boundary is oriented edge–on. Fig. 5 shows (110) twin of aragonite with its [110] direction aligned vertically, along the beam direction (*red* line). From this orientation we can see that the twin boundary is inclined with respect to electron beam. The upper domain (D1) generates the regular [110] diffraction pattern. However, as the beam crosses the twin boundary, it enters the second (lower) domain (D2) in oblique [17/9 1/9 0] projection, which

† Fractions are rounded to smallest integer numbers, so that the application of **T** transforms the unit cell of aragonite to a quasi–identical, pseudo–orthorhombic unit cell of twin domain with a=4.943 Å, b=7,993 Å, c=5.743 Å, γ=89.78°.

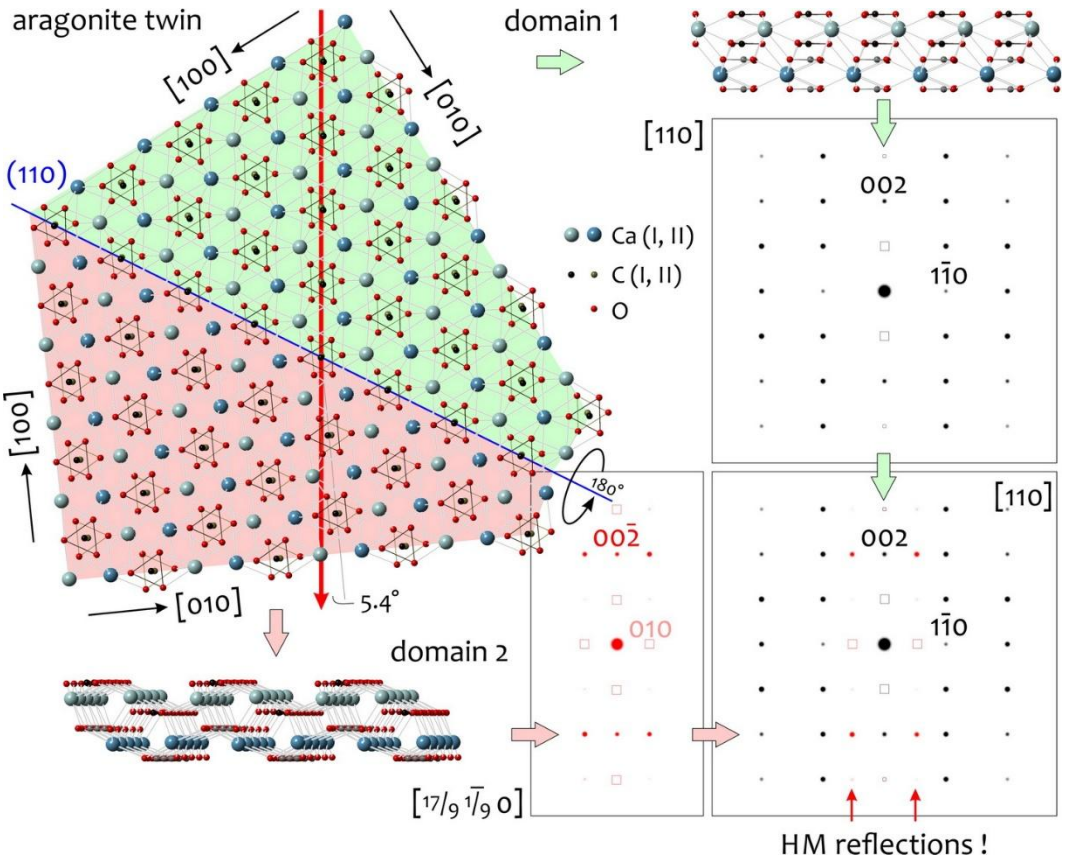


Fig. 5: **Aragonite (110) twin according to the Bragg model,[2] viewed in [001] projection**. [110] direction of the upper domain is oriented parallel to the electron beam (*red* vertical arrow). In this projection, the twin boundary (*blue* line) that separates the upper domain 1 (D1 – *green*) from the lower domain 2 (D2 – *red*) is inclined with respect to the incident electron beam. When crossing the twin boundary, following the relation in Eq. 1, the electron beam traverses the lower domain D2 along an oblique [$^{17}/_{9}$ $^{1}/_{9}$ 0] projection, just 5.4° away from the [100] projection of aragonite. The projections of twin–related domains (indicated by block arrows), as seen along the beam direction, are shown with corresponding diffraction patterns. A simple addition of the two patterns produces the apparent HM reflections. Squares denote the positions of forbidden reflections.

gives rise to a set of new reflections ignited at the halfway of {$h\bar{h}l$} of the D1 pattern. Half–integer reflections in D1 can be calculated by D2 · **T'**$^{-1}$**.** For example, 010 reflection in D2 translates into the ½½0 reflection in D1, *etc*. As illustrated in Fig. 5, these reflections stem from the 0*kl* reflection condition of the twin domain D2, explaining the common co–occurrence of [110] and [100] projections, as shown in Fig. 4. An overlay of kinematic diffraction patterns calculated separately for the first (D1) and the second (D2) domain, shown in the lower–right side of Fig. 5, demonstrates that (110) twin boundary that is present in the crystal foil could produce the HM reflections in aragonite. The orientations for selected low–index projections of aragonite domains related by twin operation (transformation matrix in Eq. 1) are listed in Table 1.

Table 1. **Twin domain orientations (D2) for selected projections of aragonite (D1)** calculated using the transformation matrix, **T** (Eq. 1) and the nearest integer projections of aragonite (D2) that could co–occur if the two domains are related by twin operation.

D1	**110**	**100**	**010**	**101**	**011**	**111**	**112**	**001**
D2	$^{17}/_{9}$ $^{1}/_{9}$ 0	$^{4}/_{9}$ $^{5}/_{9}$ 0	$^{13}/_{9}$ –$^{4}/_{9}$ 0	$^{4}/_{9}$ $^{5}/_{9}$ 1	$^{13}/_{9}$ –$^{4}/_{9}$ 1	$^{17}/_{9}$ $^{1}/_{9}$ 1	$^{17}/_{9}$ $^{1}/_{9}$ 2	001
$\bar{D}$2	100	110	3$\bar{1}$0	112	3$\bar{1}$2	201	101	001

The above described geometry corresponds to the conditions for double diffraction, a phenomenon, where a diffracted beam in upper domain is further scattered in the next, twin–related domain, producing extra diffraction spots.[58] Generated diffraction conditions depend on the orientation of the crystal and the specific crystallographic relationship between the domains. As a result, extra diffraction spots similar to those observed in <110> projections, *cf.* Fig. 1, and unusual contrast feature reminiscent of superstructures in HRTEM images, as shown in Fig. 3 are observed. These features may easily lead to erroneous interpretation of phase composition.[59]

2.4. **Twin domains approximated by twin–based polytypes**.

A simple addition of kinematic diffraction patterns, as shown in Fig. 5, however, does not properly address the complexity of electron scattering through inclined twin domains. To examine whether the apparent half–integer reflections in [110]–type projections are truly caused by out–of–plane twin domains, diffraction patterns should be calculated for a realistic twin boundary. The most proper way to do this would be to simulate realistic electron scattering across inclined twin domains, as shown in Fig. 5. On the other hand, all current methods for simulation of dynamic scattering through crystals (Bloch–wave or multislice) require periodic phase objects,[58] and nonperiodic twin model, such as shown in Fig. 5, would not be suitable for calculations.

To overcome a problem of nonperiodic twin boundary, we constructed twin–based polytypes to emulate polysynthetic twinning, and make it possible to simulate multiple scattering through inclined twin domains in selected aragonite projections. The polytypes were constructed following the same rules as for the HM–polytype by incrementing the number (n = 2, 3, *etc*.) of aragonite layers (n) between the adjacent (110) twin planes. Prior to simulations of diffraction patterns, the constructed supercells were optimized by means of DFT calculations. Details on quantum chemical calculations are described in the Materials and methods section. During optimization the regular structure of aragonite within the slabs remained roughly unchanged with some out–of–plane perturbations within the Ca layers and aplanarity of the CO_3 groups in the range of 0.07–0.12 Å along the crystallographic c–axis. The CO_3 groups adjacent to twin boundaries were symmetrized (Appendix, Fig. A3), as predicted by Makovicky (2012).[6] To simulate electron diffraction patterns, a plane wave of electrons was dynamically scattered through the twin–based polytype in selected projections using the multislice method.[58] To study the effect of inclined twin boundaries on the intensity of the diffracted beams, we selected projections where (110) twin boundary is inclined with respect to the incident electron beam. While all the polytypes with $n \geq 3$ produced half–integer reflections, the best results were obtained with DFT relaxed n = 7 polytype, which most faithfully reproduced experimental beam intensities.

The hypothetical n = 7 polytype of aragonite, that is used for simulation of dynamic scattering of electrons through inclined twin domains is shown in Fig. 6. Similar to the (110) twin model in Fig. 5, where the central domain (D1) of the polytype is oriented in [110] projection, the second domain (D2), related by twin operation, is oriented along [$^{17}/_{9}$ $^{1}/_{9}$ 0] projection of aragonite; *i.e.* [$1\bar{3}0$] projection of the twin–based n = 7 supercell. This gives rise to the formation of HM reflections in calculated diffraction patterns, as shown on the right panel of Fig. 6. The simulated diffraction patterns perfectly match experimental diffraction patterns along with the apparent HM reflections. In addition to matching of the relative intensities of reflections, the splitting of diffraction spots, characteristic for low crystal thicknesses, is reproduced. With increasing thickness, the diffraction spots merge due to dynamic recombination and produce an impeccable single–phase pattern leaving no trace about the nonconservative origin of the reflections. The splitting is indicative of the overlapping *hhl* and 0*kl* reflections of aragonite that are dynamically averaged to central positions in thick crystals. Depending on the width of respective twin domain that dominates the pattern, this gives rise to apparent 'walking' of diffraction spots (*see* Appendix, Fig. A2)

between the two reflection conditions, which makes it difficult to distinguish between the [110] projection with HM reflections *vs*. the [100] projection of aragonite.[9,18,24,49]

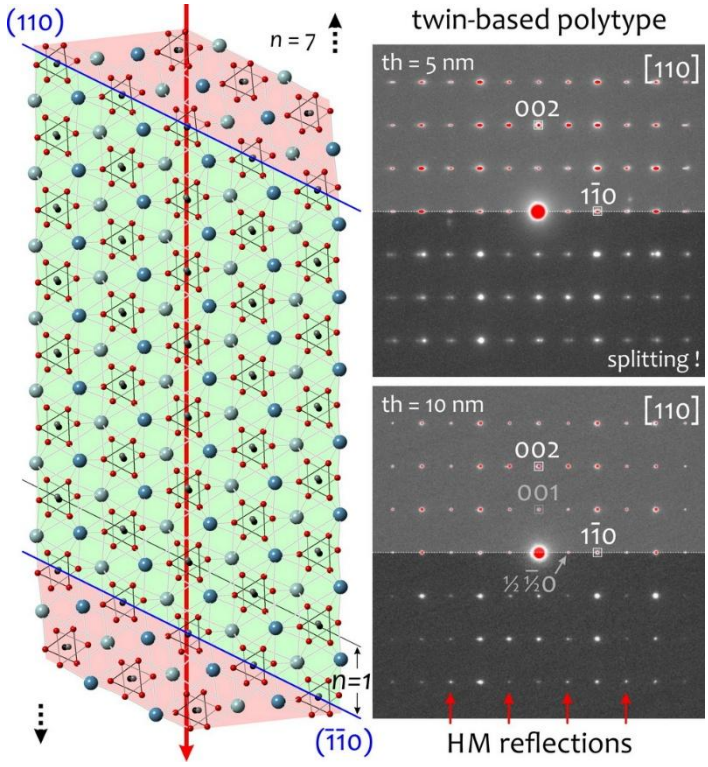


Fig. 6: **Twin–based *n*=7 polytype, an approximate of polysynthetic twinning** (*blue* lines) in aragonite for simulations of dynamic scattering through twin domains (D1 – *green* and D2 – *red*). The central domain (*green*) is oriented so that [110] projection of aragonite, *i.e.* [130] of the *n*=7 supercell is aligned vertical and parallel to the incident electron beam (*red* line). Experimental SAED patterns from two crystal thicknesses (5 and 10 nm) showing half–integer HM reflections (*red* arrows) in [110] projection, are overlaid by simulated diffraction patterns based on the *n*=7 polytype (*upper* half, *red* dots). Note the splitting of reflections (experimental and simulated) at 5 nm thickness.

The relationship between aragonite (A) and the *n* = 7 polytype (P) can be written as:

$$\mathrm{A}\cdot\mathbf{P}=\mathrm{P}\ ;\mathbf{P}=\begin{pmatrix} 1/14 & 1/14 & 0 \\ 2/7 & -5/7 & 0 \\ 0 & 0 & 1 \end{pmatrix} \qquad (2)$$

where **P** is the transformation matrix linking the two structures. Using this matrix any crystallographic projection of A can be transformed into an equivalent projection of the *n* = 7 polytype, P. For example, if we want to know the orientation of P so that one of its domains is oriented in [110] projection of A, the resulting orientation for the *n* = 7 polytype would be [$^1/_7$ $^{-3}/_7$ 0], *etc*. The list of orientations for selected low–index orientations of aragonite (A) related to the n = 7 polytype (P) via the transformation matrix **P** are listed in Table 2.

Table 2. **The relationship between aragonite** (A) **and the *n*=7 polytype** (P) of aragonite by Eq. 2 for studying the effect of twin boundaries on diffracted intensities in selected projections. Fractional indices are written as integer indices in P '.

A	**110**	**100**	**010**	**101**	**011**	**111**	**112**	**001**
P	$^1/_7$ $^{-3}/_7$ 0	$^1/_{14}$ $^2/_7$ 0	$^1/_{14}$ $^{-5}/_7$ 0	$^1/_{14}$ $^2/_7$ 1	$^1/_{14}$ $^{-5}/_7$ 1	$^1/_7$ $^{-3}/_7$ 1	$^1/_7$ $^{-3}/_7$ 2	001
P '	1$\bar{3}$0	140	1 $\overline{10}$ 0	1 4 14	1 $\overline{10}$ 14	1$\bar{3}$1	1$\bar{3}$2	001

2.5. **Journey from [110] to [001] projection – a tilting experiment**

Simulation of electron diffraction through inclined twin domains in previous section suggests that the HM reflections could be caused by intrinsic twinning of aragonite. The ultimate proof, however, would be to show experimentally, that HM reflections actually result from twinning. The best way to verify if inclined twin boundaries cause half–integer reflections in aragonite is tilting the area of interest from [110] projection that shows HM reflections into [001] projection, and confirm, whether or not this particular section contains a twin boundary. Such experiment necessitates a high–angle tilting TEM holder and a suitable crystal, oriented with the [110] projection near one end of the tilt axis to allow 90° leap from [110] to [001] projection.

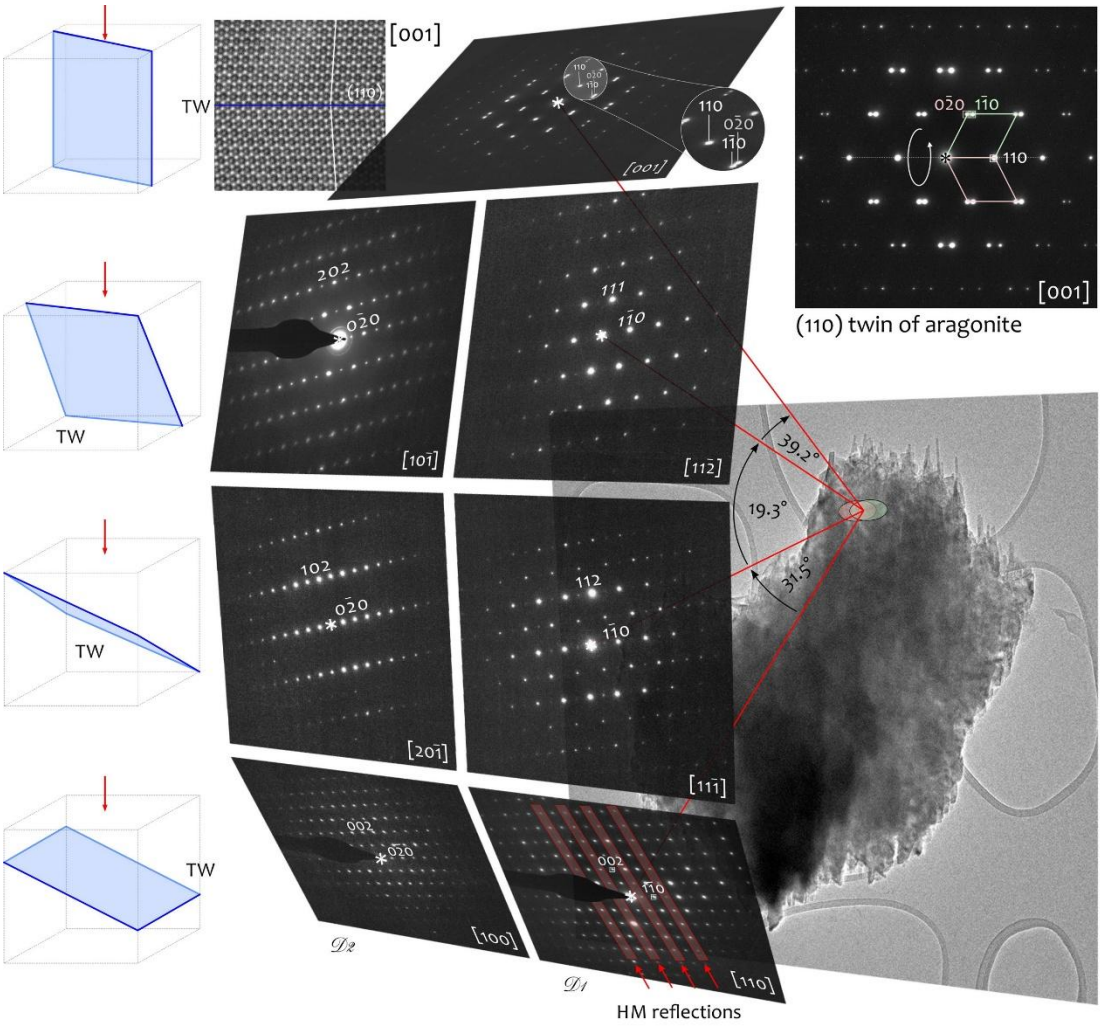


Fig. 7: **Selected area electron diffraction patterns from twinned aragonite** crystal along {$h\bar{h}$0} Kikuchi band from [110] projection, showing HM reflections, to [001] projection. HM reflections in starting [110] pattern are indicated by *red* arrows. Along with diffraction patterns from the primary domain (D1), patterns from the accompanying secondary domain (D2) are recorded with small tilt deviations according to (110) twin operation. Indicated tilt angles refer to the tilting of the primary domain. Drawings on the *left* show the relative orientation of the twin boundary (TW) with respect to the electron beam. After a full 90° tilt, a [001] pattern with characteristic twin reflections is obtained. They stem from the (110) twin of aragonite – lattice image at the *top–left side* of the figure – confirming that the true origin of HM reflections is the intrinsic twinning of aragonite.

Once the experiment is set, first diffraction pattern of [110] projection with HM reflections is recorded. In the vicinity of the HM condition of selected domain, a neighboring domain in [100] projection is observed, as shown in Fig. 4, indicating a mutual relation between the two domains

following the twin relationship written in Eq.1. From this projection the crystal is tilted along the $\{h\bar{h}0\}$ Kikuchi band of the primary domain (D1) toward [001] zone axis. If we follow this band, the primary domain (D1) goes from [110], $[11\bar{1}]$, $[11\bar{2}]$ into [001] zone axes, whereas the secondary domain (D2) is met in oblique projections, which are only few degrees away from the $\{0\bar{k}0\}$ Kikuchi band, along which this twin–related domain passes from [100], $[20\bar{1}]$, $[10\bar{1}]$ and finally merges with the primary domain in [001] zone axis. The tilting experiment is illustrated in Fig. 7. The tilt angles listed in Fig. 7 are related to the primary domain, whereas the secondary domain needed a few degrees of extra tilt to shown projections. After 90° tilt both domains constitute a characteristic twin pattern with ~6° splitting between $1\bar{1}0$ and $0\bar{2}0$ reflections. The projections that were identified in tilting experiment exactly correspond to the projection pairs as predicted by Eq. 1 and listed in Table 1. The results of tilting experiment, along with the dynamically simulated diffraction patterns using an n = 7 twin–based polytype as a twin model, demonstrate that the HM reflections factually originate from intrinsic twinning of aragonite.

2.6. **The effect of intrinsic twinning on diffraction patterns in other projections**

Given the fact that intrinsic twinning presents an irregularity in the crystal lattice, it can be expected that in addition to generating new diffraction conditions, such as half–integer reflections in ⟨110⟩–type projections, twinning would be expected to affect the resultant structure factors in other orientations as well. These effects may include changes in the relative intensities of existing diffraction conditions, as well as the ignition of space group–forbidden reflections. To study these effects we recorded diffraction patterns in selected low–index projections with intensity distributions atypical for pure aragonite. Although deviations from the regular reflection intensities have been observed before, they could not be assigned to any known cause so far.

Studying aragonite in TEM we often observe diffraction patterns with intensity peaks at positions that should be systematically extinct in *Pmcn*. They are ubiquitous in all types of samples considered in our study, regardless of their chemical purity, and are equally common in geological, synthetic or biogenic samples. For example, synthetic samples that contain no other cation except Ca, display the same frequency of patterns with notable intensity on forbidden reflections, *i.e.* (001) as the most striking example (shown in Fig. 1c), along with HM reflections, as the chemically impure aragonites of geological origin. Fig. 8 shows this effect in four sets of experimental and simulated diffraction patterns for selected low–index projections: [100] (a–d), [010] (e–h), [101] (i–l) and [011] (m–p). The differences in other low–index projections are not as striking as those in [110] zone axis with HM reflections. Nevertheless, they are unusual, and can not be interpreted by regular aragonite. Similarly, as we have composed a diffraction pattern of two twin related domains (D1 + D2) according to Eq. 1, this is done here for other low index projections in Figs. 8(b–n). with respect to the primary domain (D1), no new diffraction condition is produced by the second domain (D2), even at forbidden reflections. The reflections of twin–related projections fairly well coincide and produce distinct diffraction patterns under dynamic scattering, represented by calculated electron diffraction patterns of n = 7 twin–based polytype in Figs. 8(c–o). In these projections no superstructure reflections are produced, only some of the forbidden reflections gain intensity. For example, 101 reflection that is forbidden in aragonite (Fig. 8f) becomes a weak, but regular reflection in the n = 7 polytype (Fig. 8g). Dynamic interactions give rise to a characteristic square–like pattern of weak dots hosted within a hexagon of strong {102} & {002} reflections that are common in both aragonite and twin–based polytype. Resulting diffraction pattern, recorded from the intrinsically twinned aragonite along [010] projection is shown Fig. 8h. Similar conditions are observed in other projections, where reflections that are forbidden in aragonite become regular reflections of intrinsically twinned aragonite. The double diffraction effect caused by the intrinsic twinning is thus reflected in electron diffraction patterns in all those projections where the twin plane is inclined, with respect to the incident electron beam. The

diffraction conditions that are produced by intrinsic twinning may be further amplified by the impurity elements, such as Sr, that break down the local symmetry.

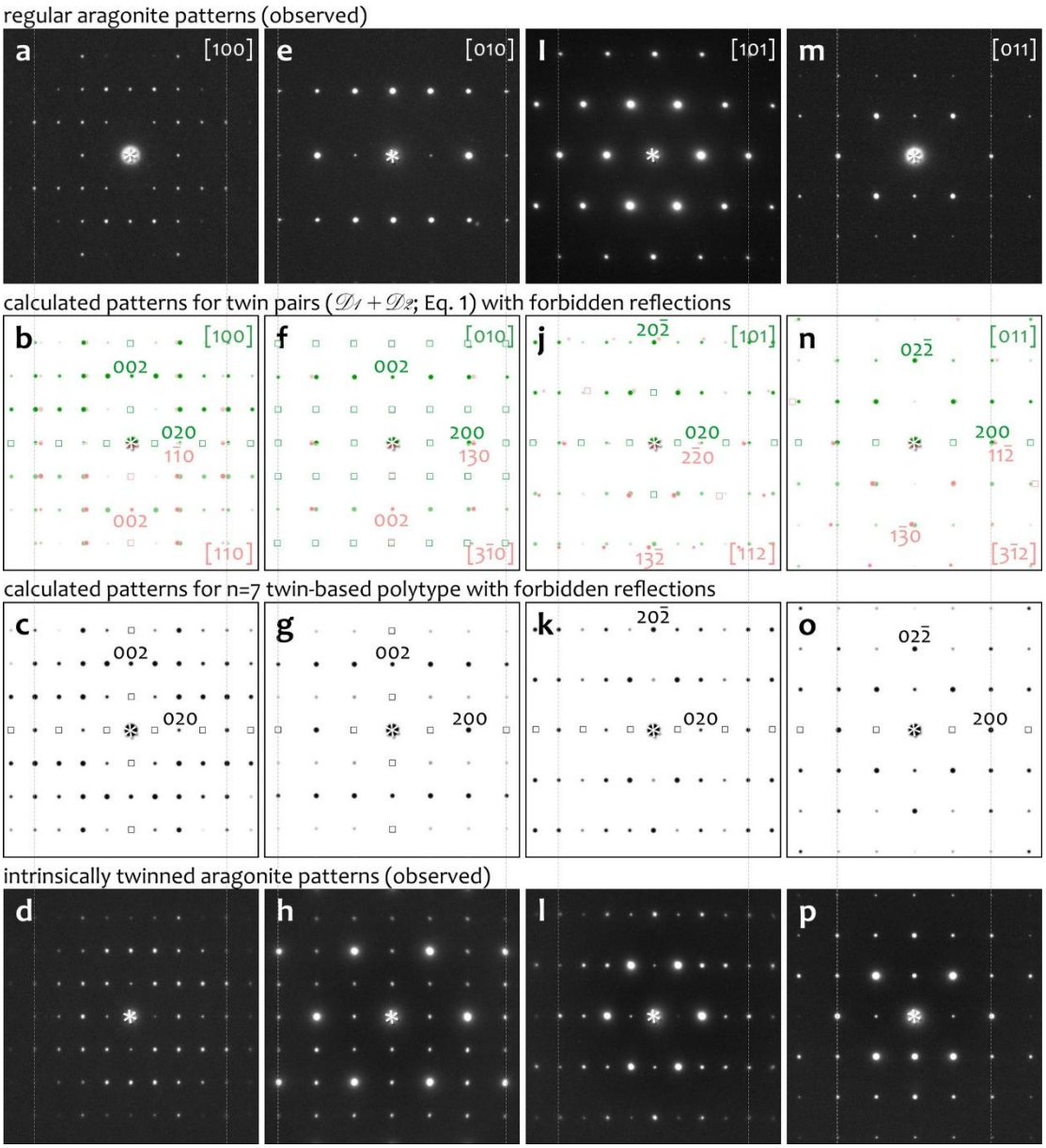


Fig. 8: **The effect of intrinsic twinning on diffraction patterns in chosen low–index zone axes**. Selected area electron diffraction patterns of untwinned (**a**–**e**–**i**–**m**) and twinned (**d**–**h**–**l**–**p**) aragonite with simulated SAED patterns for twinned aragonite domains (**b**–**f**–**j**–**n**) (D1–*green*; D2–*red*) and twin–based (n = 7) polytype model (**c**–**g**–**k**–**o**) calculated for aragonite projections: [100] (**a**–**d**), [010] (**e**–**h**), [101] (**i**–**l**) and [011] (**m**–**p**). The *squares* in simulated diffraction patterns present space group forbidden reflections. Note that some reflections that are present in twinned aragonite are forbidden in regular, untwinned aragonite. Calculated patterns in **c**–**g**–**k**–**o** match well the experimental diffraction patterns of intrinsically twinned aragonite in **d**–**h**–**l**–**p**.

Double diffraction is not as uncommon as it is often misinterpreted. Our results are in line with conclusions made by Beavan *et al.* (2002),[3] who suggested that unusual appearance of forbidden reflections could be related to the intrinsic twinning. A further evidence of this effect is an exciting debate about a similar phenomenon known in martensitic steels, where one group of authors passionately defends the existence of a controversial omega–phase,[59] whereas another group desperately demonstrates that the observed superstructure reflections are nothing but diffraction

artifacts caused by nanoscale twinning of the material.[60] Similar diffraction artifacts were reported by Larsson & Christy (2008)[61] in the study of calcite twins (*ibid*. Figs. 4c–d). Faint spurious reflections in their study were explained by superposition of [$1\bar{1}0$] and [001] domains, suggesting their relation by (104) twin operation. By establishing a clear link between twin geometry, electron scattering, and emergent diffraction features, we provide a general framework (Appendix, Figure A3) for distinguishing genuine structural complexity from artifacts arising from polysynthetic twinning. Beyond the aragonite structural specifics, our study has direct implications for phase identification in all nanoscale twinned materials and highlights the need for inclusion of twin–related phenomena in the interpretation of diffraction data.

3. **Conclusions**

Unusual diffraction conditions observed in low–temperature aragonites were studied in geological, biogenic, speleothem, and synthetic samples. Regardless of the type and chemical purity of the sample, half–integer and space–group forbidden reflections are regularly observed in all samples. The following conclusions have been made:

(1) While *Pcab* polytype of aragonite seems a plausible explanation for the observed half–integer reflections, this polytype has never been confirmed in [001] projection of aragonite neither by electron diffraction patterns nor lattice images.

(2) Intimate relation between [110] and [100] projections of aragonite in the regions where spurious reflections are observed indicate that these are two (110) twin related domains with inclined twin boundary. Electron diffraction patterns through so oriented twin domains produce apparent superstructure reflections alluding to the *Pcab* phase.

(3) False diffraction conditions stem from double diffraction effect produced by electron scattering through twin related domains in non–edge–on projections.

Beyond resolving the aragonite superstructure paradox, this study demonstrates that nanoscale twinning can produce systematic and reproducible diffraction artifacts that are easily misinterpreted as evidence for new phases. Such phenomena are not limited to aragonite, but are expected in a wide range of materials prone to polysynthetic twinning, including ceramics, semiconductors, and diverse metal and alloy systems.

4. **Experimental Section**

To best represent different origins of aragonite samples we investigated: (*i*) geological aragonite from Tazouta (Sefrou, Morocco), Enguídanos (Cuenca, Spain), Koge–Dava (Tuva, Russia) and Bazsi, Veszprém, Hungary), (*ii*) biogenic aragonite from sagittal otolith of a pike perch (*Sander lucioperca*) (*iii*) a lake sediment aragonite from Berger Károly cave (Tapolca, Hungary), and (*iv*) laboratory–synthesized aragonite nanocrystals.

Sample description and sample preparation: Geological aragonites typically occur in form of needles elongated along the crystallographic c–axis or thick pseudo–hexagonal crystals forming concentric clusters. In both types, the crystals are interpenetration twinned in {110} planes. Aragonite from Sefrou occurs in clusters of penetration twinned pseudo–hexagonal prismatic crystals with flat basal faces and twin domains grown from the common center. The samples from this locality have already been used in prior studies.[10, 19, 43] Aragonite from Cuenca occurs in simple prismatic pseudo–hexagonal crystals and as those from Sefrou, all are interpenetration twinned.[11] In contrast, the aragonite crystals from Tuva and Bazsi form aggregates of acicular crystals perched in basalt vugs. Bazsi aragonite displays the late–stage development of interpenetration

twinned prismatic pseudo–hexagonal crystals similar to those from Cuenca and Sefrou. For transmission electron microscopy (TEM) study the central parts of crystals that contain the highest density of twins were used. The speleothem sample of aragonite was collected from Titkok Tava Lake drill core in the Berger Károly cave, where it forms at 20–25 °C, in a subaqueous environment.[62] Geological and speleothem samples were prepared in two ways, in a case of macroscopic crystals as cross–sections along selected crystallographic planes following the conventional TEM sample preparation procedures, or powders deposited on lacey carbon–coated TEM grids in case of fine crystalline material. The biogenic aragonite analyzed in this study was obtained from the archived sagittal otolith samples of pike perch (Sander lucioperca) provided by the Lake Balaton Limnological Research Institute (Tihany, Hungary), which collected the samples approximately 10 years ago as part of a separate environmental monitoring program (OTKA No. T46222). For our study the fish otolith sample was embedded into a two–component Gatan epoxy resin, cut perpendicular to the longest axis of the otolith and fixed onto a TEM grid. The central part of the sample was thinned by Ar^+ ion–milling (UniMill, Technoorg–Linda Ltd, Budapest, Hungary) with an energy of 4 keV. Synthetic aragonite nanocrystals were precipitated at room temperature from Mg–rich aqueous solutions. In this procedure,[63] 20 ml of 0.01 M Na_2CO_3 buffer solution was first prepared from double distilled MilliQ water and mixed with 20 ml of 0.01 M $CaCl_2$ and 0.04 M $MgCl_2$ solutions without any pH adjustment. The vessels were closed and the precipitated materials were matured for 4 weeks. The end–product of the aging was filtered through a 0.45 μm MCE membrane filter using a vacuum pump and washed by 20 ml MilliQ water. After filtering the product was deposited on lacey C–coated TEM grids.

Transmission electron microscopy: TEM studies were carried out on microscopes operated at the accelerating voltage of 200 kV; an FEI Talos FX200–G2 scanning TEM (Nanolab, University of Pannonia), and conventional and high–resolution TEMs Jeol 2100 and 2010F (Center for Electron Microscopy, Jožef Stefan Institute). Selected area electron diffraction (SAED) patterns and bright–field (BF) TEM images were recorded using a built–in CCD camera. SAED patterns obtained in tilting experiment were recorded using a sample holder with a 160° tilt range.

Construction of twin and twin–based polytypes: Structure models of (110) twins and twin–based polytype structures in aragonite were constructed to study superstructure reflections. To build the models we used the structure data from Ye *et al*. (2012),[64] where aragonite structure is refined in the orthorhombic space group *Pmcn* (62) with unit cell parameters a = 4.962 Å, b = 7.963 Å, and c = 5.743 Å. Using structure modeling software (CrystalMaker® Software Ltd., Oxfordshire, UK)[65] (110) twin boundary was constructed in a geometry as proposed by Suzuki *et al*. (2012),[25] except that in our notation the supercell's C–axis is set parallel to the c–axis of aragonite, whereas its A–axis is normal to the (110) twin pane. In this twin model, CO_3 groups are located at the twin plane, as proposed by Bragg (1924).[2] Accordingly, the super–cells possess the following orientation relationship with aragonite: $\vec{A} = (\vec{a}\cdot\vec{b}^2 + \vec{b}\cdot\vec{a}^2)/(\vec{a}^2 + \vec{b}^2)$, $\vec{B} = (\vec{b} - \vec{a})$, $\vec{C} = \vec{c}$. Owing to twin operation supercells with single twin boundary would be nonperiodic along the A–axis. To overcome discontinuity problems the supercells with complementary interfaces are constructed.[66] According to this procedure, the primary twin boundary is placed at the center of the A–axis. Periodicity along the A–axis is then obtained by cutting the A–dimension by n (110) slabs on each side of the twin plane. As a result, a complementary twin boundary with identical local structure is generated at the A–terminations. Such double twin boundary models that are now periodic along the A–axis and can be used for reciprocal space computations that rely on periodic lattices. Their A–dimension depends on the number (n) of (110) slabs separating the twin planes, while B and C are constant for all supercells: $A = 2n\cdot d_{(110)}(4.221\ Å)\ |_{n=1,2,3,..}$, $B = \sqrt{[d_{(100)}^2 + d_{(010)}^2]}(9.382\ Å)$, and $C = d_{(001)}(5.743\ Å)$. Depending on the number (n) of (110) slabs series of twin–based polytypes are obtained where the shortest polytype of this series with just one (110) slab (n=1) on each side of the twin boundary corresponds to the iconic *Pcab* polytype, with A = 8.42 Å, as proposed by Hiragi

et al. (1966)[5] and Makovicky (2012)[6]. Depending on *n*, the supercells thus contain 40, 80, 120, .. atoms. A twin–based supercell is illustrated in Appendix, Fig A4. In addition to twin–based polytypes, *mAra* supercells in a $P2_1/c$ space group with a = 28.6 Å, b = 5.7 Å, c = 9.2 Å, and β= 120.2(5)°, according Neméth *et al*. (2019),[8] were constructed for comparison. Crystal Cracker software (K. Leinenweber, Arizona State Univ., USA) was used for matrix–based cell transformations among aragonite and twin–based polytypes. The supercells were symmetrized within the *Pcab* space group using the FindSym® code (ISOTROPY Software Suite, Brigham Young University, Provo, Utah 84602, USA).[67] To ignite forbidden reflections in aragonite and twin–based superstructures, Ca atoms were replaced by Sr at random positions to satisfy the formal composition of aragonite measured by EDS. Rigid super–cells were then used in first principles calculations and calculations of dynamic electron scattering.

First principle calculations and calculations of diffraction patterns: Density functional theory (DFT) was used for full structure relaxation of twin–based polytypes. The calculations have been performed with the VASP code, using a plane wave basis set and the projector augmented wave (PAW) method.[68] Exchange–correlation effects were taken into account in generalized gradient approximation (GGA) by the Perdew–Burke–Ernzerhof (PBE) functional.[69] The Brillouin zone was sampled with k–point grid of $2\pi*0.035Å^{-1}$ within the Monkhorst–Pack scheme.[70] After relaxation, the kinematic diffraction patterns were calculated using the SingleCrystal suite of CrystalMaker® software,[65] and simulations of dynamic scattering of electrons was based on the Multislice method were performed using the JEMS package (P.A. Stadelmann, EPFL).[58]

Statistical analysis: Distribution of (110) twins, unrelated to the sample origin, varies from high density with SFs and twin planes at *n* = 2, 3, .. 7, 8, *etc*. to low density with twin plane separations of 50 nm or more. They occur in two sets of {110} planes, where one typically dominates, whereas the other type appears within individual domains alongside SFs.[13] HM reflections and space–group forbidden reflections are more common in densely twinned regions. When measuring d–values from SAED patterns planar projection distortions due to the placement of the CCD camera with respect to the incident electron beam must be taken into account. Such distortions are measured from elliptical deformation of SAED ring patterns of Au nanoparticles on C–coated TEM grid. In our case we measured a y–axis distortion of 1.4 %, which has been taken into account in geometrical correction of SAED patterns prior to analysis. In DFT calculations the cutoff energy for the plane wave basis set was chosen at 400 eV. An iterative relaxation of atomic positions was stopped when the sum of all forces acting on each atom were smaller than 0.02 eV/Å.

Acknowledgements

The authors are grateful for the access to the microscope facilities to the Center for Electron Microscopy at the Jožef Stefan Institute in Ljubljana (Slovenia) and the Nanolab Center of the Research Institute of Biomolecular and Chemical Engineering in Veszprém (Hungary). The access to supercomputer facilities of the IGM SB RAS (Novosibirsk) is gratefully acknowledged.

Funding

This study is part of the research project 'Aragonite structure and formation', supported by Slovenian–Hungarian bilateral research grants:

Slovenian Research Agency (ARIS):

- Grant No. N1–0230 (AR, VR, PNG)
- Grant No. Z2–50056 (VR)

National Office of Research, Development and Innovation of Hungary (NKFIH):

- Grant No. SNN–139585 (MP, ZM, PN, PNG).
- Grant No. RRF–2.3.1–21–2022–00014 (MP, ZM, PP)
- Grant No. ANN141894 (PN)

IGM SB RAS State Assignment; Grant No. 122041400157–9 (PNG).

This study has received extra funding from the Europe research and innovation program (EU Horizon) under a grant agreement No. 101131765 (EXCITE2) and from NKFIH (2020–2.1.1–ED–2023–00254) for Transnational Access at Nanolab, University of Pannonia (AR, MP).

Author Contributions

The question on superstructure reflections in aragonite was first raised by P.N.G., who initiated the topic studied in this paper. A.R. first identified half–integer reflections in mineralogical aragonite samples from Spain and Morocco. M.P. identified the half–integer reflections in a fish–otolith sample, P.N. in speleothems, and Z.M. in synthetic aragonite. V.R. explained the origin of half–integer reflections by intrinsic twinning of aragonite and designed models for simulations. P.P. conducted the high–angle tilting experiment, that proved, that half–integer reflections stem from intrinsic twins. P.N.G and P.N. calculated transformation matrices and I.D. calculated structure factors for twin–based polytype structures to simulate the dynamic scattering through twin domains. The paper was written by V.R. and A.R. with contributions of all authors.

Conflicts of Interest

There are no conflicts to declare.

Data Availability Statement

Any supporting data and measurement information from this study, including the structure models, are available upon reasonable request from the corresponding author.

Keywords

aragonite, {110} twinning, double diffraction, polytypes, DFT calculations

References

[1] James NP, Jones B. *Origin of Carbonate Sedimentary Rocks*, John Wiley and Sons 2016, 19–21.

[2] Bragg WL. *The structure of aragonite*, Proceedings of the Royal Society of London Series A **105**/729 (1924) 16–39. DOI: 10.1098/rspa.1924.0002

[3] Bevan DJM, Rossmanith E, Mylrea DK, Ness SE, Taylor MR, Cuff C. *On the structure of aragonite – Lawrence Bragg revisited*, Acta Crystallographica B **58**/3 (2002) 448–456. DOI: 10.1107/s0108768102003294

[4] Caspi E, Pokroy B, Lee P, Quintana J Zolotoyabko E. *On the structure of aragonite*. Acta Crystallographica B **61**/2 (2005) 129–132. DOI: 10.1107/S0108768105005240

[5] Hiragi Y, Kachi S, Takada T, Nakanishi N. *The superstructure in fine aragonite particles*, Bulletin of the Chemical Society of Japan **39**/11 (1966) 2361–2364. DOI: 10.1246/bcsj.39.2361

[6] Makovicky E. *Twinning of aragonite – the OD approach*, Mineralogy and Petrology **106**/1–2 (2012) 19–24. DOI: 10.1007/s00710-012-0219-5

[7] Gillet P, Gérard Y, Willaime C. *The calcite–aragonite transition: Mechanism and microstructures induced by the transformation stresses and strain*. Bulletin de Minéralogie **110**/5 (1987) 481–496. DOI: 10.3406/bulmi.1987.7992

[8] Németh P, Mugnaioli E, Gemmi M, Czuppon G, Demény A, Spötl C. *A nanocrystalline monoclinic CaCO 3 precursor of metastable aragonite*. Science Advances **4**/12 (2018) eaau6178. DOI: 10.1126/sciadv.aau6178.

[9] Gavryushkin PN, Rečnik A, Daneu N, Sagatov N, Belonoshko AB, Popov ZI, Ribić V, Litasov KD. *Temperature induced twinning in aragonite: transmission electron microscopy experiments and ab initio calculations*. Zeitschrift Für Kristallographie **234**/2 (2018) 79–84. DOI: 10.1515/zkri-2018-2109.

[10] Gavryushkin PN, Belonoshko AB, Sagatov N, Sagatova D, Zhitova E, Krzhizhanovskaya MG, Rečnik A, Alexandrov EV, Medrish IV, Popov ZI, Litasov KD. *Metastable structures of $CaCO_3$ and their role in transformation of calcite to aragonite and postaragonite*. Crystal Growth & Design **21**/1 (2020) 65–74. DOI: 10.1021/acs.cgd.0c00589.

[11] Richards RP. *An Examination of Classic Twinning in Aragonite*. Rocks & Minerals ; **96**/5 (2021) 454–459. DOI: 10.1080/00357529.2021.1848221.

[12] Immenhauser A, Hoffmann R, Riechelmann S, Mueller M, Scholz D, Voigt S, et al. *Petrographic and geochemical constraints on the formation of gravity-defying speleothems*. The Depositional Record **9**/3 (2022) 413–436. DOI: 10.1002/dep2.199.

[13] Gavryushkin PN, Rečnik A, Donskikh KG, Banaev MV, Sagatov NE, Rashchenko S, et al. *The intrinsic twinning and enigmatic twisting of aragonite crystals*. Proceedings of the National Academy of Sciences **121**/6 (2024) e2311738121. DOI: 10.1073/pnas.2311738121.

[14] Mutvei H. *Ultrastructural Characteristics of the Nacre in Some Gastropods*. Zoologica Scripta **7**/1–4 (1978): 287–296. DOI: 10.1111/j.1463-6409.1978.tb00612.x.

[15] Marsh ME, Sass RL. *Aragonite Twinning in the Molluscan Bivalve Hinge Ligament*. Science **208**/4449 (1980) 1262–1263. DOI: 10.1126/science.208.4449.1262.

[16] Liu J, Sarikaya M, Aksay IA. *A hierarchically structured model composite: A tem study of the hard tissue of red abalone*. Materials Research Society: Mat. Res. Soc. Symp. Proc. **255** (1992) 10–17.

[17] Checa AG, Ramírez-Rico J, González-Segura A, Sánchez-Navas A. *Nacre and false nacre (foliated aragonite) in extant monoplacophorans (=Tryblidiida: Mollusca)*. Naturwissenschaften **96**/1 (2008) 111–122. DOI: 10.1007/s00114-008-0461-1.

[18] Benzerara K, Meibom A, Gautier Q, Kaźmierczak J, Stolarski J, Menguy N, et al. *Nanotextures of aragonite in stromatolites from the quasi-marine Satonda crater lake, Indonesia*. Geological Society, London, Special Publications **336**/1 (2010) 211–224. DOI: 10.1144/sp336.10.

[19] Kogure T, Suzuki M, Kim H, Mukai H, Checa AG, Sasaki T, et al. *Twin density of aragonite in molluscan shells characterized using X-ray diffraction and transmission electron microscopy*. Journal of Crystal Growth **397** (2014) 39–46. DOI: 10.1016/j.jcrysgro.2014.03.029.

[20] Kudo M, Kameda J, Saruwatari K, Ozaki N, Okano K, Nagasawa H, et al. Microtexture of larval shell of oyster, Crassostrea nippona: A FIB–TEM study. Journal of Structural Biology 169 (2010) 1–5. DOI: 10.1016/j.jsb.2009.07.014.

[21] Suzuki M, Kameda J, Sasaki T, Saruwatari K, Nagasawa H, Kogure T. *Characterization of the multilayered shell of a limpet, Lottia kogamogai (Mollusca: Patellogastropoda), using SEM–EBSD and FIB–TEM techniques*. Journal of Structural Biology **171** (2010) 223–230. DOI: 10.1016/j.jsb.2010.04.008.

[22] Mukai H, Saruwatari K, Nagasawa H, Kogure T. *Aragonite twinning in gastropod nacre*. Journal of Crystal Growth **312**/20 (2010) 3014–3019. DOI: 10.1016/j.jcrysgro.2010.07.002.

[23] Yokoo N, Suzuki M, Saruwatari K, Aoki H, Watanabe K, Nagasawa H, et al. *Microstructures of the larval shell of a pearl oyster, Pinctada fucata, investigated by FIB–TEM technique*. American Mineralogist **96**/7 (2011) 1020–1027. DOI: 10.2138/am.2011.3657.

[24] Hayashi A, Yokoo N, Nakamura T, Watanabe T, Nagasawa H, Kogure T. *Crystallographic characterization of the crossed lamellar structure in the bivalve Meretrix lamarckii using electron beam techniques*. Journal of Structural Biology **176**/1 (2011) 91–96. DOI: 10.1016/j.jsb.2011.06.011.

[25] Suzuki M, Kim H, Mukai H, Nagasawa H, Kogure T. *Quantitative XRD analysis of {110} twin density in biotic aragonites*. Journal of Structural Biology **180**/3 (2012) 458–468. DOI: 10.1016/j.jsb.2012.09.004.

[26] Checa AG, Mutvei H, Osuna-Mascaró AJ, Bonarski JT, Faryna M, Berent K, et al. *Crystallographic control on the substructure of nacre tablets*. Journal of Structural Biology **183**/3 (2013) 368–376. DOI: 10.1016/j.jsb.2013.07.014.

[27] Griesshaber E, Schmahl WW, Ubhi HS, Huber J, Nindiyasari F, Maier B, et al. *Homoepitaxial meso- and microscale crystal co-orientation and organic matrix network structure in Mytilus edulis nacre and calcite*. Acta Biomaterialia **9**/12 (2013) 9492–9502. DOI: 10.1016/j.actbio.2013.07.020.

[28] Wang SN, Yan XH, Wang R, Yu DH, Wang XX. *A microstructural study of individual nacre tablet of Pinctada maxima*. Journal of Structural Biology **183**/3 (2013) 404–411. DOI: 10.1016/j.jsb.2013.07.013.

[29] Zhang J, Yan J, Sheng J. *Nanoscale structure and formation mechanism of the aragonite fibers in the ligament of Hyriopsis Cumingii shell*. Journal of Materials Science **50**/9 (2015) 3383–3390. DOI: 10.1007/s10853-015-8894-3.

[30] Almagro Í, Drzymała P, Rodríguez-Navarro AB, Sainz-Díaz CI, Willinger MG, Bonarski J, et al. *Crystallography and Textural Aspects of Crossed Lamellar Layers in Arcidae (Bivalvia, Mollusca) Shells*. Key Engineering Materials **672** (2016) 60–70. DOI: 10.4028/www.scientific.net/kem.672.60.

[31] Willinger MG, Checa AG, Bonarski JT, Faryna M, Berent K. Biogenic *Crystallographically Continuous Aragonite Helices: The Microstructure of the Planktonic Gastropod Cuvierina*. Advanced Functional Materials **26**/4 (2015) 553–561. DOI: 10.1002/adfm.201504034.

[32] Shin YA, Yin S, Li X, Lee S, Moon S, Jeong J, Kwon M, Yoo SJ, Kim YM, Zhang T, Gao H, Oh SH. *Nanotwin-governed toughening mechanism in hierarchically structured biological materials*. Nature Communications **7** (2016) 10772. DOI: 10.1038/ncomms10772.

[33] Zhang J, Yan J, Sheng J. *Nanoscale structure and formation mechanism of the aragonite fibers in the ligament of Hyriopsis Cumingii shell*. Journal of Materials Science **50**/9 (2015) 3383–3390. DOI: 10.1007/s10853-015-8894-3.

[34] He J, Zhao S, Wei Z, Bismayer U. *Mesoscale twinning in shells of Pinctada martensii*. Zeitschrift Für Kristallographie **231**/11 (2016) 673–680. DOI: 10.1515/zkri-2016-1989.

[35] Chen G, Luo H, Luo S, Lin Z, Ma Y. *Vertically oriented structure and its fracture behavior of the Indonesia white-pearl oyster*. Journal of the Mechanical Behavior of Biomedical Materials **66** (2017) 211–223. DOI: 10.1016/j.jmbbm.2016.11.002.

[36] Liu J, Huang Z, Pan Z, Wei Q, Li X, Qi Y. *Atomistic Origin of Deformation Twinning in Biomineral Aragonite*. Physical Review Letters **118**/10 (2017) 105501. DOI: 10.1103/physrevlett.118.105501.

[37] Ji HM, Li XW, Chen DL. *Crystallographic texture of crossed-lamellar structure in Cymbiola nobilis shell*. Journal of the Ceramic Society of Japan **125**/5 (2017) 419–422. DOI: 10.2109/jcersj2.16333.

[38] Agbaje OBA, Wirth R, Morales LFG, Shirai K, Kosnik M, Watanabe T, et al. *Architecture of crossed-lamellar bivalve shells: The southern giant clam (Tridacna derasa, Röding, 1798)*. Royal Society Open Science 4/9 (2017) 170622. DOI: 10.1098/rsos.170622.

[39] Jacob DE, Ruthensteiner B, Trimby P, Henry H, Martha SO, Leitner J, et al. *Architecture of Anoteropora latirostris (Bryozoa, Cheilostomata) and implications for their biomineralization*. Scientific Reports **9**/1 (2019) 11439. DOI: 10.1038/s41598-019-47848-4.

[40] Otter LM, Agbaje OBA, Kilburn MR, Lenz C, Henry H, Trimby P, et al. *Insights into architecture, growth dynamics, and biomineralization from pulsed Sr–labelled Katelysia rhytiphora shells (Mollusca, Bivalvia)*. Biogeosciences **16**/17 (2019) 3439–3455. DOI: 10.5194/bg-16-3439-2019.

[41] Crippa G, Griesshaber E, Checa AG, Harper EM, Simonet Roda M, Schmahl WW. *Orientation patterns of aragonitic crossed-lamellar, fibrous prismatic and myostracal microstructures of modern Glycymeris shells*. Journal of Structural Biology **212**/3 (2020) 107653. DOI: 10.1016/j.jsb.2020.107653.

[42] Deng Z, Jia Z, Li L. Biomineralized Materials as Model Systems for Structural Composites: *Intracrystalline Structural Features and Their Strengthening and Toughening Mechanisms*. Advanced Science **9**/14 (2022) 2103524. DOI: 10.1002/advs.202103524.

[43] San X, Gong M, Wang J, Ma X, dos Reis R, Smeets PJM, et al. *Uncovering the crystal defects within aragonite $CaCO_3$*. Proceedings of the National Academy of Sciences **119**/4 (2022) e2122218119. DOI: 10.1073/pnas.2122218119.

[44] Shindo H, Kwak M. *Stabilities of crystal faces of aragonite ($CaCO_3$) compared by atomic force microscopic observation of facet formation processes in aqueous acetic acid*. Physical Chemistry Chemical Physics **7**/4 (2005) 691–696. DOI: 10.1039/b417384h.

[45] Liu F, Gao Y, Zhao S, Shen Q, Su Y, Wang D. *Biomimetic fabrication of pseudohexagonal aragonite tablets through a temperature-varying approach*. Chemical Communications **46**/25 (2010) 4607–4609. DOI: 10.1039/b925593a.

[46] Sand KK, Rodriguez-Blanco JD, Makovicky E, Benning LG, Stipp SLS. *Crystallization of $CaCO_3$ in Water–Alcohol Mixtures: Spherulitic Growth, Polymorph Stabilization, and Morphology Change*. Crystal Growth & Design **12**/2 (2011) 842–853. DOI: 10.1021/cg2012342.

[47] Koga N, Kasahara D, Kimura T. *Aragonite Crystal Growth and Solid-State Aragonite–Calcite Transformation: A Physico–Geometrical Relationship via Thermal Dehydration of Included Water*. Crystal Growth & Design **13**/5 (2013) 2238–2246. DOI: 10.1021/cg400350w.

[48] Willinger MG, Polleux J, Antonietti M, Cölfen H, Pinna N, Nassif N. *Structural evolution of aragonite superstructures obtained in the presence of the siderophore deferoxamine*. CrystEngComm **17**/21 (2015) 3927–3935. DOI: 10.1039/c5ce00186b.

[49] Yu SH, Li H, Yao QZ, Fu SQ, Zhou GT. *Hierarchically nanostructured shuttle-like aragonite mesocrystals: Preparation, characterization, growth mechanism, and removal ability to La(III)*. Journal of Environmental Chemical Engineering **5**/1 (2017) 893–905. DOI: 10.1016/j.jece.2017.01.004.

[50] Aquilano D, Pastero L, Bruno M. *Adsorption/Absorption of Lithium Affecting the Growth Morphology of Aragonite. The Two–Dimensional Epitaxy of Li_2CO_3 (Zabuyelite) on the {001} Form of Aragonite ($CaCO_3$)*. Crystal Growth & Design **19**/7 (2019) 3969–3978. DOI: 10.1021/acs.cgd.9b00375.

[51] Puthanveettil RK, Lee Y, Heo J, Kim MJ. *Morphological control of $CaCO_3$ superstructures in seawater: Insights into Ca–source anion influence and formation mechanism*. Advanced Powder Technology **34**/12 (2023) 104249. DOI: 10.1016/j.apt.2023.104249.

[52] Molnár Z, Pekker P, Rečnik A, Pósfai M. *Formation and properties of spindle-shaped aragonite mesocrystals from Mg–bearing solutions*. Nanoscale 16/4 (2024) 2012–2021. DOI: 10.1039/d3nr04672a.

[53] Massaro FR, Bruno M, Rubbo M. *Surface structure, morphology and (110) twin of aragonite*. CrystEngComm **16**/4 (2014) 627–635. DOI: 10.1039/c3ce41654b.

[54] Marzouki MA, Souvignier B, Nespolo M. *Twinning of aragonite – the crystallographic orbit and sectional layer group approach*. Acta Crystallographica A **71**/2 (2015) 195–202. DOI: 10.1107/s2053273314027156.

[55] Mugnaioli E, Gorelik TE. *Structure analysis of materials at the order–disorder borderline using three-dimensional electron diffraction*. Acta Crystallographica B **75**/4 (2019) 550–563. DOI: 10.1107/s2052520619007339.

[56] Škundrić T, Zagorac D, Zarubica A, Matović B. *Theoretical investigation of mollusk shells: Energy landscape exploration of $CaCO_3$ polymorphs and element substitution: A short review*. Advanced Technologies **10**/7 (2021) 73–80. DOI: 10.5937/savteh2101073s.

[57] Aquilano D, Bruno M, Ghignone S, Pastero L. *Twinning and homoepitaxy cooperation in the already rich growth morphology of $CaCO_3$ polymorphs*. I. Aragonite. Journal of Applied Crystallography **56**/6 (2023) 1630–1638. DOI: 10.1107/s1600576723008208.

[58] Stadelmann PA. *EMS – A software package for electron diffraction analysis and HREM image simulation in materials science*. Ultramicroscopy **21**/2 (1987) 131–145. DOI: 10.1016/0304-3991(87)90080-5.

[59] Ping D. *Review on ω phase in body-centered cubic metals and alloys*. Acta Metallurgica Sinica 27/1 (2014) 1–11. DOI: 10.1007/s40195-013-0014-2.

[60] Cayron C. *Diffraction artefacts from twins and stacking faults, and the mirage of hexagonal, polytypes or other superstructures*. Scripta Materialia **194** (2021) 113629. DOI: 10.1016/j.scriptamat.2020.11.014

[61] Larsson A–K, Christy AG. *On twinning and microstructures in calcite and dolomite*. American Mineralogist **93** (2008) 103–113. DOI: 10.2138/am.2008.2520.

[62] Demény A., Berentés A., Rinyu L., Kovács I., Surányi G., Virág M. *Subaqueous carbonate speleothems as paleotemperature archives – clumped isotope thermometry and stable isotope compositions of inclusion–hosted water*. International Journal of Speleology **53**/1 (2024) 25–37. DOI: 10.5038/1827-806X.53.1.2480

[63] Molnár Z, Pekker P, Dódony I, Pósfai M. *Clay minerals affect calcium (magnesium) carbonate precipitation and aging*. Earth and Planetary Science Letters **567** (2021) 116971. DOI: 10.1016/j.epsl.2021.116971.

[64] Ye Y, Smyth JR, Boni P. *Crystal structure and thermal expansion of aragonite-group carbonates by single-crystal X-ray diffraction*. American Mineralogist **97**/4 (2012) 707–712. DOI: 10.2138/am.2012.3923.

[65] Palmer DC. *Visualization and analysis of crystal structures using CrystalMaker software*. Zeitschrift Für Kristallographie **230**/9–10 (2015) 559–572. DOI: 10.1515/zkri-2015-1869.

[66] Ribić V, Jordan V, Drev S, Kovač J, Dražić G, Rečnik A. *Mnemonic rutile–rutile interfaces triggering spontaneous dissociation of water*. Advanced Materials **36** (2024) 2308027. DOI: 10.1002/adma.202308027

[67] Stokes HT, Hatch DM. *FINDSYM: program for identifying the space-group symmetry of a crystal*. Journal of Applied Crystallography **38**/1 (2005) 237–238. DOI: 10.1107/s0021889804031528.

[68] Kresse G, Joubert D. *From ultrasoft pseudopotentials to the projector augmented–wave method*. Physical Review B **59**/3 (1999) 1758–1775. DOI: 10.1103/PhysRevB.59.1758.

[69] Perdew JP, Burke K., Ernzerhof M. *Generalized gradient approximation made simple*. Physical Review Letters **77**/18 (1996) 3865–3868. DOI: 10.1103/PhysRevLett.77.3865.

[70] Monkhorst H J, Pack JD. *Special points for Brillouin–zone integrations*. Physical Review B **13**/12 (1976) 5188–5192. DOI: 10.1103/PhysRevB.13.5188.

Appendix

Appendix A1: **Comparison between aragonite and a hypothetical *Pcab* polytype**.[5,6]

As shown in the Introduction of this paper, the two–layered Hiragi–Makovicky polytype, based on intrinsic (110) twinning of aragonite, produces the puzzling superstructure reflections in [1$\bar{1}$0] projection. This polytype, however, has never been observed in [001] projection of aragonite. The diffraction patterns for [001] projection of both aragonite and the hypothetical *Pcab* polytype are shown in Fig. S1.

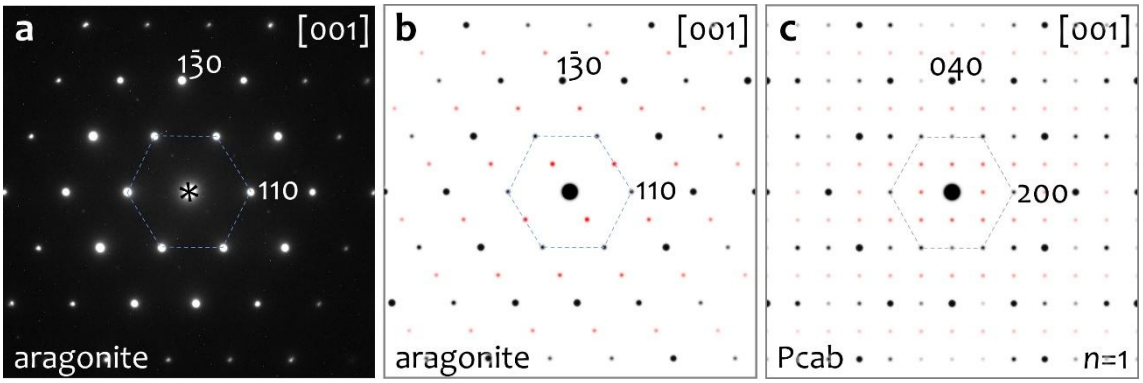


Fig. A1. Electron diffraction patterns in [001] projection of aragonite. (**a**) usual experimental diffraction pattern with no forbidden reflections, (**b**) calculated diffraction pattern with forbidden reflections (*red*), and (**c**) calculated diffraction pattern of 2–layered *Pcab* polytype of aragonite, proposed by Hiragi *et al*. (1966)[5] and Makovicky (2012),[6] with forbidden reflections (*red*).

While [001] diffraction patterns with or without space group forbidden reflections (Figs. A1a–b) are commonly observed in aragonite samples, the [001] pattern of the hypothetical *Pcab* polytype (Fig. A1c) has not been identified in any samples in this study. This pattern could be mistaken by the more common [010] pattern of twinned aragonite, shown in Fig. 8h, but the corresponding reciprocal d–values in the [001] pattern of the *Pcab* are ~25% smaller.

Appendix A2: **'Walking' reflections.**

In electron microscopy studies of aragonite the discrepancies in the interpretations of the zone axes are common. This is due to so–called 'walking' reflections caused by an intrinsic twinning of aragonite. The most characteristic example of this diffraction artifact is [100]–[110] pair of projections that are related by {110} twin operation (Table 1, main text). The phenomenon is demonstrated in Fig. A2.

Owing to inexplicable extra reflections, [110] projection with (h+½ k+½ l) superstructure reflections is often mistaken by [100] projection with forbidden (0 k 2l)$|_{k=odd}$ reflections due to similar c/a ratio. Besides weak superstructure or forbidden reflections two projections display quite characteristic differences in intensity distribution that make them unique (Figs. A2a and A2c). In [100] projection we observe intermittent rows of forbidden (0 k 2l) reflections due to dynamic scattering, while in [110] projection we observe rows of half–integer (½h ½k l) reflections. Slightly out of zone axes, the intensity maxima walk between c/l = 0.69 and 0.73, which are characteristic values for [100] and [110] projections, respectively, confusing researchers to interpret DPs as either of the two zone axes.[23] This effect is demonstrated in Fig. A2b, where individual DPs between two diffraction conditions are recorded and summed up to show the lateral c/l transition.

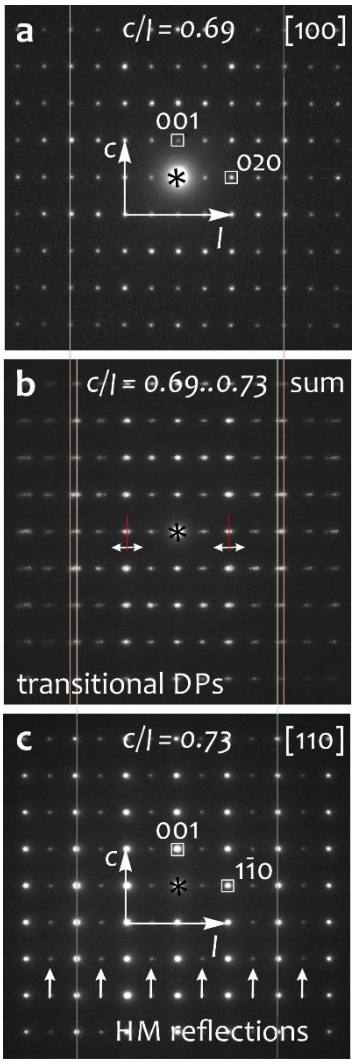


Fig. A2. Transitional diffraction conditions as observed between [100] and [110] zone axes of intrinsically twinned aragonite samples. (**a**) pure [100] projection, (**b**) intermediate 'walking' reflections, and (**c**) [110] projection with HM reflections characteristic of intrinsic twinning.

Appendix A3: **Criteria to distinguish Twin-induced artifacts from true Superstructures**.

Our work establishes a generalizable framework for identifying and interpreting diffraction artifacts in intrinsically twinned materials. The proposed scheme is based on the principle that inclined twin interfaces can generate additional reflections through double diffraction, which closely mimic genuinely new phases or superstructures. Our protocol combines crystallographic analysis of twin relationships, superstructure violations along twin edge–on orientations, identification of coexisting zone axes, and verification by tilting experiments and simulations. Particular attention should be paid to reflections that appear only in specific orientations, and shift or 'walk' with crystal thickness or tilt, which is characteristic of overlapping twin-related domains. Simulations based on twin-derived supercell approximations provide the key criterion for distinguishing the artifacts from the true superstructures. The scheme is generally applicable to twinned ceramics, minerals, semiconductors, and metallic systems where nanoscale twinning complicates true phase identification (Figure A3: Practical criteria).

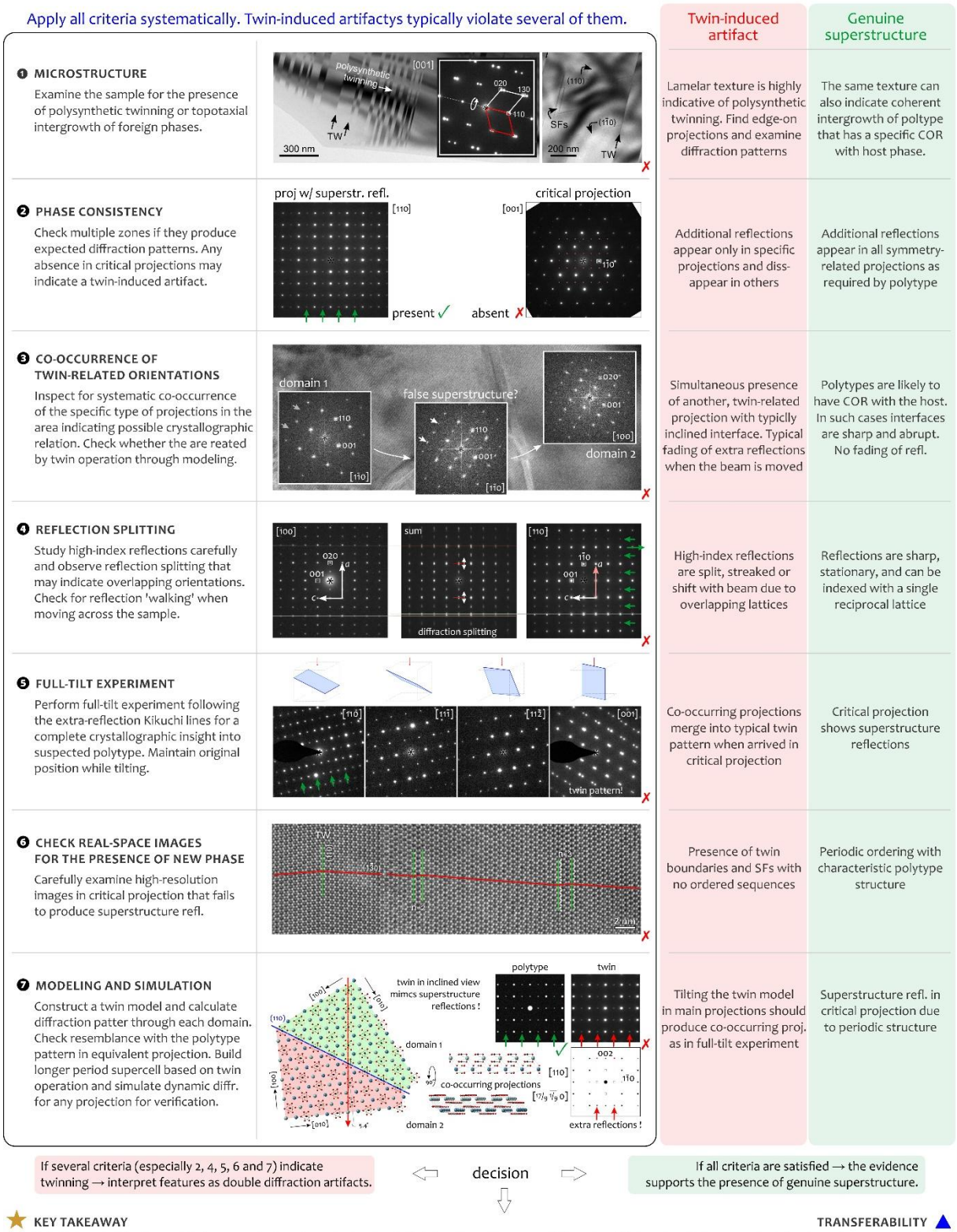


Fig. A3. Practical criteria to distinguish twin–induced diffraction artifacts from true superstructures.

Appendix A4: **Supercell setting of twin–based *Pcab* polytypes**.

According to Bragg (1926),[2] (110) twin of aragonite is generated by 180° rotation around the (110)–plane normal on selected CO_3 plane. While Bragg has not specified how exactly the model was constructed, the twin operation can be deduced from the translations in Ca–sublattice and positions of the triangular CO_3 groups. Implementing the above twin operation, series of twin–based polytypes can be constructed based on obverse and reverse twinning following a selected number of (110) layers (*n* = 1,2,3 ..) of aragonite structure, as illustrated in Fig. A4 below.

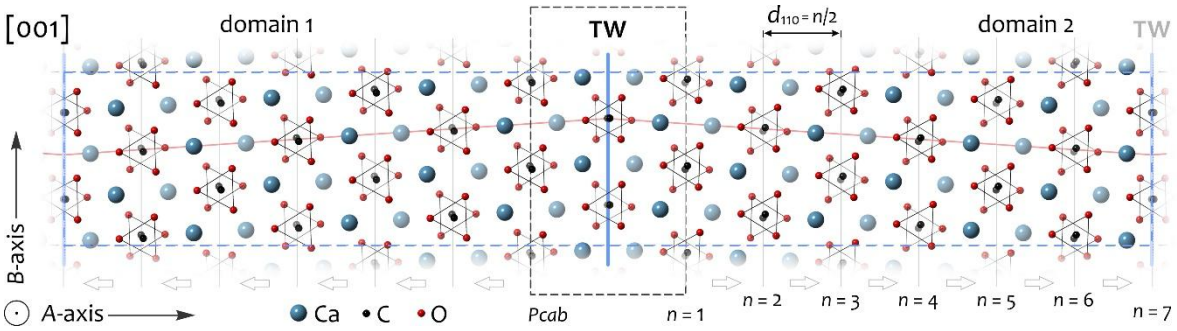


Fig. A4. Geometrical setting of twin–based polytype supercells for DFT calculations.

In this study, polytypes of the *n* = 1, 2, 3 .. series were used to simulate the diffraction conditions caused by intrinsic twinning of aragonite. The structures were optimized by first principles calculations by means of DFT. Due to twin operation all polytypes converge into the *Pcab* space group. All polytypes show a local symmterization of the CO_3 groups across the twin plane (*i.e.* horizontal across the TW plane, tilted in bulk aragonite). This effect is most pronounced in the shortest period polytype *n* = 1, corresponding to Hiragi–Makovicky polytype (*see* Introduction),[5,6] and fades away with the distance from the twin plane.